Modulation of the Southern Africa Precipitation Response to the El Niño Southern Oscillation by the Subtropical Indian Ocean Dipole

Andrew Hoell[1]

NOAA Earth System Research Laboratory Physical Sciences Division

Chris Funk

Department of Geography University of California Santa Barbara

U.S. Geological Survey

Jens Zinke

Institut für Geologische Wissenschaften, Freie Universität Berlin

Department of Environment and Agriculture, Curtin University of Technology

Australian Institute of Marine Science

School of Geography, Archaeology and Environmental Studies, University of Witwatersrand

Laura Harrison

Department of Geography University of California Santa Barbara

23 May 2016

[1] Corresponding Author Address: Andrew Hoell, NOAA/ESRL/PSD, 325 Broadway, Boulder, CO 80305, email: andrew.hoell@noaa.gov

Abstract

The climate of Southern Africa, defined as the land area bound by the region 15°S-35°S; 12.5°E-42.5°E, during the December-March rainy season is driven by Indo-Pacific sea surface temperature (SST) anomalies associated with the El Niño Southern Oscillation (ENSO) and the Subtropical Indian Ocean Dipole (SIOD). The observed December-March 1979-2014 Southern Africa precipitation during the four ENSO and SIOD phase combinations suggests that the phase of the SIOD can disrupt or enhance the Southern Africa precipitation response to ENSO. Here, we use a large ensemble of model simulations driven by global SST and ENSO-only SST to test whether the SIOD modifies the relationship between Southern Africa precipitation and ENSO. Since ENSO-based precipitation forecasts are used extensively over Southern Africa, an improved understanding of how other modes of SST variability modulate the regional response to ENSO is important.

ENSO, in the absence of the SIOD, forces an equivalent barotropic Rossby wave over Southern Africa that modifies the regional mid-tropospheric vertical motions and precipitation anomalies. El Niño (La Niña) is related with high (low) pressure over Southern Africa that produces anomalous mid-tropospheric descent (ascent) and decreases (increases) in precipitation relative to average. When the SIOD and ENSO are in opposite phases, the SIOD compliments the ENSO-related atmospheric response over Southern Africa by strengthening the regional equivalent barotropic Rossby wave, anomalous mid-tropospheric vertical motions and anomalous precipitation. By contrast, when the SIOD and ENSO are in the same phase, the SIOD disrupts the ENSO-related atmospheric response over Southern Africa by weakening the regional equivalent

barotropic Rossby wave, anomalous mid-tropospheric vertical motions and anomalous precipitation.

1. Introduction

The climate of Southern Africa, defined as the land area bound by the region 15°S-35°S; 12.5°E-42.5°E, is related with the spatial variations of Pacific, Indian and Atlantic Ocean sea surface temperatures (SST) (e.g. Nicholson and Kim 1997). The Indo-Pacific Ocean SST anomaly expressions related to Southern Africa climate have been shown to be a consequence of three modes of SST variability: The El Niño Southern Oscillation (ENSO) (e.g. Nicholson and Entekhabi 1986) shown in Fig. 1a, the Indian Ocean Dipole (IOD) (Saji and Yamagata 2003) shown in Fig. 1b and the Subtropical Indian Ocean Dipole (SIOD) (Behera et al. 2000, Behera and Yamagata 2001, Reason 2001, Washington and Preston 2006) shown in Fig. 1c. In this manuscript, we examine how modes of Indo-Pacific SST variability simultaneously force Southern Africa precipitation during the December-March rainy season.

On average, ENSO events force atmospheric circulations over Southern Africa that result in regional precipitation anomalies (e.g. Nicholson and Entekhabi 1986, Lindesay 1988, Jury et al. 1994, Rocha and Simmonds 1997, Nicholson and Kim 1997, Reason et al 2000, Misra 2003). A mid-tropospheric convection dipole between the region that includes the eastern Indian Ocean and Maritime Continent and the central Pacific Ocean during ENSO events excites Rossby waves over Southern Africa (Ratnam et al. 2014, Hoell et al. 2015) that modifies the regional moisture fluxes (Reason and Jagadheesha 2005, Hoell et al. 2015) and vertical motions (Hoell et al. 2015) thereby forcing the regional precipitation (Nicholson and Kim 1997). On average, canonical El Niño (La Niña), forces high (low) pressure anomalies over Southern Africa, which in turn forces anomalous reductions (increases) in moisture fluxes, anomalous downward (upward) vertical motions and decreases (increases) in precipitation relative to average.

There is considerable inter-event variability in the Atlantic and Indo-Pacific SST (Wrytki 1975) and the atmospheric teleconnections driven by those SST over Southern Africa between each El Niño and La Niña (Ratnam et al. 2014, Hoell et al. 2015). Alone, Atlantic SST as a result of 'Benguela El Nino' have been shown to influence Southern Africa climate (Rouault et al. 2003, Hansingo and Reason 2009). Atlantic SST in concert with Indian Ocean SST modify the El Niño and La Niña-forced atmospheric teleconnections over Southern Africa during December-March (Nicholson 1997, Goddard and Graham 1999). Observational analyses have suggested that atmospheric teleconnections during La Niña are more sensitive to SST forcing over the Atlantic Ocean while atmospheric teleconnections during El Niño are more sensitive to SST forcing over the Indian Ocean (Nicholson and Kim 1997). Problematically, the differences in the pattern and magnitude of SST anomalies between seemingly similar El Niño or La Niña events can compromise the potential predictability of Southern Africa precipitation. For example, the strength and position of the Angola low is different from one ENSO event to the next, which is the reason for the lack of the expected severe drought during the 1997-1998 El Niño (Reason and Jagadheesha 2005, Lyon and Mason 2009). Therefore, we reexamine the critical role that Indian Ocean SSTs play in modifying the ENSO-driven Southern Africa precipitation during December-March. December-March is the height of the Southern Africa rainy season and is the time of year in which Southern Africa is most sensitive to ENSO (Manatsa et al. 2015).

Indian Ocean SST variability on seasonal to interannual time scales is largely expressed in the form of dipole patterns across the ocean basin as a result of the SIOD (Behera et al. 2000, Behera and Yamagata 2001) whose SST expression is shown in Fig. 1c and the IOD (e.g., Chambers et al, 1999; Webster et al, 1999; Saji et al, 1999) whose SST expression is shown in Fig. 1b. The SST anomaly expression of the SIOD (Fig. 1c) forces atmospheric circulations over Southern Africa that modifies the flux of moisture and therefore precipitation (Reason 2001, Washington and Preston 2006). The SST anomaly expression of the IOD (Fig. 1b) forces wide-ranging teleconnections across the Indian Ocean basin and surrounding areas by modifying the zonal winds (Saji et al. 1999), moisture fluxes over Africa (Behera et al. 2005) and precipitation over Southern Africa (Saji and Yamagata 2003).

The relative effects of Indian Ocean SST and Pacific Ocean SST on Southern Africa climate are currently unknown. Manatsa (2011a, 2012) attempted to decouple the effect of the IOD and ENSO on the leading components of Southern Africa rainfall using observational data. Manatsa (2011a, 2012) had limited success due to what appeared to be changes in the behavior of the atmospheric circulation during the 1970s and 1990s. However, what is known is that atmospheric models forced by Indian Ocean and Pacific Ocean SST more accurately depict the climate of Southern Africa as compared to the forcing by Pacific SST alone (Reason and Jagadheesha 2005). Therefore, understanding the simultaneous effects of Indo-Pacific SST on Southern African climate is important.

The global SST anomaly pattern related to the observed December-March 1979-2014 Southern Africa precipitation variability is shown in Fig. 2b. The observed Southern Africa precipitation (Fig. 2a) is related with an SST anomaly pattern (Fig. 2b) that features characteristics of ENSO (Fig. 1a) and the SIOD (Fig. 1c). The SST anomaly expression of the IOD (Fig. 1b) is unrelated with historical Southern Africa precipitation during December-March (Fig. 2b). Enhanced Southern Africa precipitation is related with La Niña, defined by a cool east-central tropical Pacific Ocean, and a positive SIOD, defined by a warm southwest Indian Ocean and cool central Indian Ocean. Reduced Southern Africa precipitation is related with El Niño, defined by a warm east-central tropical Pacific Ocean, and a negative SIOD, defined by a cool southwest Indian Ocean and a warm central Indian Ocean. Overall, the observed Southern Africa precipitation is most closely related to opposing phases of ENSO and the SIOD (Fig. 2b).

Observed conditions during 1979-2014 indicate that differences in the simultaneous phasing of ENSO and the SIOD (Table 1) results in precipitation anomalies of varying strength over Southern Africa during December-March (Fig. 3). When ENSO and the SIOD were out of phase, Southern Africa precipitation was strongly reduced during El Niño (Fig. 3a-b) and Southern Africa precipitation was strongly enhanced during La Niña (Fig. 3e-f). By contrast, when ENSO and the SIOD were in phase, Southern Africa precipitation was only marginally reduced during El Niño (Fig. 3c-d) and Southern Africa precipitation was only marginally enhanced during La Niña (Fig. 3g-h). The observed December-March 1979-2014 Southern Africa precipitation during the four ENSO and SIOD phase combinations suggests that the phase of the SIOD can disrupt or enhance the Southern Africa precipitation response during ENSO.

In this manuscript, we examine how the phase of the SIOD, and therefore the SST anomaly expression of the Indian Ocean, modulates the Southern Africa precipitation response to ENSO through comparisons of two large atmospheric simulation ensembles for 1979-2014. The first ensemble is forced by global SST variability, which includes the combined effects of ENSO and the SIOD, and the second ensemble is forced by SST variability associated only with ENSO. We test the degree to which the SIOD modulates the ENSO-related precipitation response over Southern Africa by comparing the historical atmospheric simulation ensembles separated by phase of the SIOD. In section 2, we describe the observed historical data and the two atmospheric simulations ensembles utilized. In section 3, we examine how the SIOD modulates the atmospheric teleconnections and precipitation associated with ENSO over Southern Africa. In section 4, we provide a summary.

2. Data, Models and Methods

2.1 Observed Data

Observed historical precipitation for 1979-2014 is from the Global Precipitation Climatology Project (GPCP) blended satellite and rain gauge estimates version 2.2 on a 2.5°x2.5° latitude-longitude fixed grid (Adler et al. 2003, Huffman et al. 2009). Observed historical SSTs for 1979-2014 are from the merged Hadley-NOAA Optimum Interpolation dataset developed by Hurrell et al. (2008) on a 1.0°x1.0° latitude-longitude fixed grid. Observed SST and sea ice concentrations from Hurrell et al. (2008) also specify the ocean boundary conditions in historical atmospheric model simulations.

2.2 Atmospheric Model Simulations

Two separate atmospheric model experiments for 1979-2014 are used to test whether the SIOD modulates the Southern Africa precipitation response to ENSO during the December-March rainy season. The two experiments are each made up of 80 ensembles, 30 of which are generated using the ECHAM5.4 model (Roeckner et al. 2006) and 50 of which are generated using the GFS version 2 model (Saha et al. 2013). The GFS version 2 is integrated on a T126 horizontal grid and 64 sigma-pressure hybrid vertical levels, and uses virtual temperature as the prognostic variable (Saha et al. 2013). The ECHAM5.4 model is integrated on a T159 horizontal grid and 31 vertical levels, and uses a spectral dynamical core in which vorticity, temperature and the logarithm of surface pressure are calculated using a spherical harmonics truncation (Roeckner et al. 2006). The GFS version 2 and ECHAM5.4 model outputs are interpolated to a 1˚x1˚ horizontal grid for comparison. The experiments are simulated for 1979-2014, thus limiting the analysis to that time period.

The first experiment is used to test the atmospheric response to the observed global SST, and is driven by time-varying historical monthly global SST, sea ice concentrations, greenhouse gas concentrations and aerosols for 1979-2014. The second experiment is used to test the atmospheric response to ENSO, and is driven by the leading pattern of global time-varying monthly SST anomaly added to the monthly climatology, observed sea ice concentrations, greenhouse gas concentrations and aerosols for 1979-2014.

The leading pattern of global SST anomaly was identified by a covariance-based empirical orthogonal function (EOF) calculation of detrended monthly SST from January 1978-December 2011 (Fig. 4). The leading pattern of SST and the experiment driven by the leading pattern of SST are hereafter referred to as EOF1. The spatial pattern of EOF1 (Fig. 4a) closely resembles the SST anomaly expression of ENSO (Fig. 1a), and the principal component of EOF1 (Fig. 4b) is correlated with the Niño3.4 index at r=0.97. For 2012-2014, the principal component of EOF1 is calculated by projecting EOF1 (Fig. 4a) on to the observed SST. The monthly SST expression related to EOF1 for 1979-2014 is obtained by multiplying EOF1 (Fig. 4a) by its principal component (Fig. 4b). The monthly SST anomaly of EOF1 is added to the 1979-2010 monthly SST climatology to obtain the time-varying monthly SST used as the ocean boundary condition of the simulations. For more information on these experiments please visit the URL http://www.esrl.noaa.gov/psd/repository/alias/facts.

2.3 Comparison of Observed and Simulated Southern Africa Precipitation

The monthly average 1979-2014 observed precipitation over Southern Africa indicates that the primary precipitation season spans December-March (Fig. 5b). December-March 1979-2014 observed precipitation over Southern Africa is unevenly distributed in space (Fig. 5a). Regionally, the greatest precipitation amounts during December-March fall over Malawi, Angola, Zambia and Mozambique while the lowest precipitation amounts fall over the Atlantic facing coastlines of southwest Southern Africa (Fig. 5a).

The monthly averaged precipitation variability of the ECHAM5.4 and GFS version 2 simulations driven by observed global time-varying SST (Fig. 5d,f) are similar to the observed precipitation (Fig. 5b), with correlations in excess of 0.98. While the correlation between the observed monthly precipitation climatology and the climatology of the simulations driven by global SST over Southern Africa are very similar, there is a dry bias in the ECHAM5.4 and GFS version 2 models of about 30% each month. Due to this dry bias we show standardized precipitation anomalies in time and space in the following analyses. Standardized precipitation anomalies are defined as the precipitation anomaly divided by the seasonal cycle standard deviation of precipitation.

The average December-March 1979-2014 precipitation of the ECHAM5.4 and GFS version 2 simulations driven by observed global time-varying SST over Southern Africa (Figs. 5c,e) are broadly similar in space to the observed precipitation (Fig. 5a). The differences in the average December-March 1979-2014 precipitation of the ECHAM5.4 (Fig. 5c) and GFS version 2 (Fig. 5e) simulations driven by observed global time-varying SST and observed precipitation are noticeable over elevated areas likely because the resolution at which the models are simulated are too coarse to capture orographic processes with sufficient detail.

The temporal variability of observed precipitation and precipitation resolved by simulations driven by global SST and EOF1 of SST over Southern Africa for December-March 1979-2014 are shown in Figs. 6a and 6b, respectively. The atmospheric model experiments capture the interannual variability and magnitude of standardized precipitation anomalies well during prolonged periods. Furthermore, the observed precipitation always falls within the 80-member ensemble spread of the atmospheric model simulations. The results presented here show that the simulations forced by global SST and EOF1 of SST capture the precipitation climatology and variability of Southern Africa well and are suitable to test the SST effects on Southern Africa.

3. Southern Africa Precipitation Sensitivity to ENSO

Fig. 7a shows the correlation of observed SST and Southern Africa precipitation variability in simulations driven by global SST for December-March 1979-2014. The simulations driven by global SST affirm the historical observed relationship between SST and Southern Africa precipitation (Fig. 2b). Southern Africa precipitation is associated with ENSO (Fig. 1a) and a southwest-to-northeast dipole of SST in the Indian Ocean similar to the SST anomaly expression of the SIOD (Fig. 1c). Simulations driven by global SST (Fig. 6a) also affirm observed historical conditions in that the IOD (Fig. 1b) is not significantly related with December-March Southern Africa precipitation.

Fig. 7b shows the correlation of observed SST and Southern Africa precipitation in simulations driven by EOF1 of SST for December-March 1979-2014 to test the degree to which ENSO alone is related with Southern Africa precipitation. The simulations driven by EOF1 once again affirm the observed historical relationship between ENSO and Southern Africa precipitation (Fig. 2b), with similar spatial correlations to the simulations driven by global SST over the central Pacific Ocean (Fig. 7a). The relationship between Indian Ocean SST and Southern Africa precipitation driven by EOF1 of SST are weak, as evidenced by weak, yet significant, correlations over the central Indian Ocean (Fig. 7b) that are present in EOF1 (Fig. 4a). The SST anomaly expression associated with Southern Africa precipitation in simulations driven by EOF1 (Fig. 7b) does not include the SST anomaly expression of the SIOD (Fig. 1c) in contrast with the simulations driven by global SST (Fig. 7a).

Since the SIOD is not fully realized in the forcing of Southern Africa precipitation by EOF1 (Fig. 7b), but is fully realized in the forcing of Southern Africa precipitation by global SST (Fig. 7a), we are able to test whether the SIOD modifies the relationship between Southern Africa precipitation and ENSO through a comparison of these two experiments. We test whether the SIOD modifies the relationship between Southern Africa precipitation and ENSO though an examination of Southern Africa precipitation as a function of SIOD phase in simulations forced by global SST and EOF1 of SST.

Fig. 8 shows the relationship between Southern Africa precipitation, SST and ENSO separated by phase of the SIOD in simulations forced by global SST. When all December-March seasons are considered, Southern Africa precipitation is associated with the SST anomaly expressions (Fig. 8a) of ENSO (Fig. 1a) and the SIOD (Fig. 1c), and is significantly correlated with the Niño3.4 index (Fig. 8b). When the Niño3.4 and SIOD indices have the opposite sign during December-March, Southern Africa precipitation is again associated with the SST anomaly expressions (Fig. 8c) of ENSO (Fig. 1a) and the SIOD (Fig. 1c), and is significantly correlated with the Niño3.4 index (Fig. 8d). The difference between the condition in which the Niño3.4 and SIOD indices have the opposite sign and when all seasons are considered is that the relationship between Southern Africa precipitation and Indo-Pacific SSTs is stronger when the Niño3.4 and SIOD indices have the opposite sign. When the Niño3.4 and SIOD indices have the same sign during December-March, Southern Africa precipitation is associated with an SST anomaly over the Agulhas Current region (Fig. 8e) that does not resemble either the ENSO (Fig. 1a) or the SIOD (Fig. 1c) SST anomaly expressions. SST anomalies in the Agulhas Current have been shown to modify the regional Southern Africa precipitation and cloud cover during December-March (Jury 1992 and Fauchereau et al. 2009).

This examination of Southern Africa precipitation as a function of the SIOD phasing indicates that the SIOD modulates the Southern Africa precipitation response to

ENSO. When the SIOD and Niño3.4 indices have the opposite sign, which results in an SST expression that closely resembles the historical SST and Southern Africa precipitation relationship (Fig. 2b), this condition results in a stronger Southern Africa precipitation response (Fig. 8). When the SIOD and Niño3.4 indices have the same sign, Southern Africa precipitation is not related to the SST anomaly expressions (Fig. 8e) of ENSO (Fig. 1a) or the SIOD (Fig. 1c). Depending on the phase of the SIOD, the effect of the SIOD can either compliment the Southern Africa precipitation response to ENSO, or can disrupt the Southern Africa precipitation response to ENSO, affirming the small sample of observed conditions (Fig. 3).

The atmospheric circulation over Southern Africa associated with ENSO and separated by phase of the SIOD during December-March in simulations forced by global SSTs is shown in Fig. 9. When all December-March seasons are considered, ENSO is related to an equivalent barotropic Rossby wave over Southern Africa, that modifies the regional mid-tropospheric vertical motions and precipitation. El Niño (La Niña) is related with high (low) pressure over Southern Africa (vectors in Fig. 9a,b) that is responsible for anomalous mid-tropospheric descent (ascent) (Fig. 9b) and decreases (increases) in precipitation relative to average (Fig. 9a). When the Niño3.4 and SIOD indices have the opposite sign during December-March, the SIOD compliments the ENSO-related atmospheric response over Southern Africa by strengthening the equivalent barotropic Rossby wave (Fig. 9c,d), anomalous mid-tropospheric vertical motions (Fig. 9d) and anomalous precipitation (Fig. 9d). When the Niño3.4 and SIOD indices have the same sign during December-March, the SIOD disrupts the ENSO-related atmospheric response over Southern Africa by weakening the equivalent barotropic

Rossby wave (Fig. 9e,f) anomalous mid-tropospheric vertical motions (Fig. 9f) and anomalous precipitation (Fig. 9e).

Fig. 10 shows the relationship between Southern Africa precipitation, SST and ENSO separated by phase of the SIOD in simulations forced by EOF1 of SST. Note that the correlations of Southern Africa precipitation are to the full SST, and not EOF1 of SST, to demonstrate that the SIOD has no effect in the simulations driven by EOF1. When all December-March seasons are considered, Southern Africa precipitation is associated with the SST anomaly expression (Fig. 10a) of EOF1 (Fig. 4a), which by design is the same as the SST anomaly expression of ENSO (Fig. 1a).

When the Niño3.4 and SIOD indices have the opposite sign during December-March, Southern Africa precipitation in simulations forced by EOF1 is related with the SST anomaly expression (Fig. 10c) of ENSO (Fig. 1a), as is expected. The SST anomaly expression of the SIOD also appears in this correlation, but only because the correlation is performed against the full SST field. The SIOD has no effect on Southern Africa precipitation in simulations driven by EOF1, as the relationship between Southern Africa precipitation and SST (Fig. 10d) is statistically indistinguishable from the aggregate case (Fig. 10b) over the tropical Pacific Ocean. This contrasts the Southern Africa precipitation in simulations driven by global SST (Fig. 8), where the relationship between Southern Africa precipitation and ENSO significantly increased from the aggregate case when the SIOD and Niño3.4 indices are in the opposite phase (Fig. 8a,c).

When the Niño3.4 and SIOD indices have the same sign during December-March, Southern Africa precipitation in simulations forced by EOF1 is again related with the SST anomaly expression (Fig. 10d) of ENSO (Fig. 1a). The southwestern dipole of the

SST anomaly expression of the SIOD appears in this correlation only because the correlation is performed against the full SST field. The SIOD has no effect on Southern Africa precipitation in simulations forced by EOF1, as the relationship between Southern Africa precipitation (Fig. 10f) is statistically indistinguishable from the aggregate case (Fig. 10b) over the tropical Pacific Ocean.

The atmospheric circulations related to ENSO over Southern Africa in simulations forced by EOF1 are also statistically indistinguishable when separated by phase of the SIOD during December-March (Fig. 11). As was discussed previously, ENSO is related to an equivalent barotropic Rossby wave over Southern Africa, that modifies the regional mid-tropospheric vertical motions and precipitation (Fig. 11).

4. Summary and Discussion

The historical ENSO and Southern Africa relationship (e.g. Fig. 2) has facilitated the successful prediction of Southern Africa precipitation during many December-March rainy seasons (e.g. Hastenrath et al. 1995). On average, La Niña is related with enhanced Southern Africa precipitation while El Niño is related with reduced Southern Africa precipitation. However, there have been historical occurrences in which La Niña events (Fig. 3g) occurred simultaneously with widespread areas of near average December-March precipitation over Southern Africa (Fig. 3h). Since the SIOD, a mode of SST variability in the Indian Ocean, is also related with Southern Africa precipitation, we examine whether the SIOD modulates the ENSO-related teleconnection over Southern Africa.

Observed historical relationships (Fig. 2) and atmospheric model simulations simulations (Fig. 7) driven by global SST for December-March 1979-2014 indicate that Southern Africa precipitation is associated with ENSO (Fig. 1a) and the SIOD (Fig. 1c). Observed historical relationships (Fig. 2) and atmospheric model simulations (Fig. 7) driven by global SST also indicate that Southern Africa precipitation during December-March is unrelated with the IOD (Fig. 1b). Enhanced Southern Africa precipitation is related to La Niña, defined by a cool east-central tropical Pacific Ocean, and a positive SIOD, defined by a warm southwest Indian Ocean and cool central Indian Ocean. Reduced Southern Africa precipitation is related to El Niño, defined by a warm east-central tropical Pacific Ocean, and a negative SIOD, defined by a cool southwest Indian Ocean and a warm central Indian Ocean. Overall, simulations driven by global SST and observed conditions indicate that Southern Africa precipitation is related to opposing phases of ENSO and the SIOD.

The average December-March 1979-2014 precipitation anomaly over Southern Africa during ENSO events in which ENSO and the SIOD were out of phase was much greater than the precipitation anomaly during ENSO events in which ENSO and SIOD were in phase (Fig. 3). Therefore, we examine whether the phase of the SIOD can modulate the relationship between ENSO and Southern Africa precipitation.

The modulation of the ENSO teleconnection over Southern Africa by the SIOD is tested through comparisons of two large atmospheric simulation ensembles for 1979-2014. The first ensemble is forced by global SST variability, which includes the combined effects of ENSO and the SIOD, and the second ensemble is forced by SST variability associated only with ENSO. We test the degree to which the SIOD modulates the ENSO-related precipitation response over Southern Africa by comparing the two large historical atmospheric simulation ensembles separated by phase of the SIOD.

Atmospheric model simulations driven by only ENSO indicate that ENSO forces an equivalent barotropic Rossby wave over Southern Africa that modifies the regional mid-tropospheric vertical motions and precipitation (Fig. 8). El Niño (La Niña) is related with high (low) pressure over Southern Africa that is responsible for anomalous mid-tropospheric descent (ascent) and decreases (increases) in precipitation relative to average.

The atmospheric model simulations affirm the observed conditions (Fig. 3) in that the SIOD can complement or disrupt the Southern Africa precipitation response to ENSO (Figs. 8 and 9). Simulations driven by global SST indicate that opposing ENSO and SIOD phases generate complimentary telconnections that result in enhanced precipitation changes over Southern Africa. By contrast, simulations driven by global SST indicate that when ENSO and the SIOD are in phase, the SIOD disrupts the ENSO-related teleconnections over Southern Africa by weakening the equivalent barotropic Rossby wave (Fig. 9f) anomalous mid-tropospheric vertical motions (Fig. 9f) and anomalous precipitation (Fig. 9e). While this work presents compelling evidence, additional experiments that isolate the effect of the Indian Ocean SST on Southern Africa climate could be examined to further confirm the SIOD and ENSO relationship implied by atmospheric model simulations driven by global SST and EOF1 of SST.

A well-established body of literature has shown that decadal variations of Southern Africa precipitation are related with the regional and global SST (Mason and Jury 1997, Reason and Rouault 2002, Allan et al 2003; Zinke et al., 2009; Grove et al., 2013). The decadal variations of precipitation and circulation over Southern Africa are 'ENSO-like' (Reason and Rouault 2002, Allan et al 2003). The results presented in this manuscript pertain only to the 1979-2014 period, and this analysis cannot speak to whether decadal and multi-decadal variations have an effect on the SIOD and ENSO relationship. Future work should focus the changing relationships between Southern Africa precipitation, ENSO and the SIOD on decadal and multi-decadal time scales.

Recent research by Reason and Smart (2015) showed that Atlantic SST anomalies in proximity to Angola and Namibia are related with Southern Africa December-March rainfall during ENSO and SIOD phase combinations. Specifically, during 2001, 2006 and 2011, strong positive Atlantic SST anomalies during La Nina and positive SIOD occurred simultaneously with widespread Southern Africa above average rainfall. Atlantic SST may have a discernable effect on Southern Africa precipitation during ENSO and SIOD phase combinations, and the sensitivity of that effect should be tested in future studies.

Early methods of rainy season Southern Africa precipitation prediction were based only upon the statistical analyses of historical climate information (e.g. Hastenrath et al. 1995). For the early statistical models, the predictors of Southern Africa precipitation included metrics of ENSO, expressed in terms SST or atmosphere-only indices such as the Southern Oscillation Index, and the atmospheric circulation. Southern Africa precipitation forecasts have evolved to include both statistical models and dynamical model forecasts simultaneously (Landman and Goddard 2005) or only dynamical model forecasts (Landman et al. 2012, Yuan et al. 2014). The recent improvements of dynamical model SST forecasts (Wang et al. 2009), which lead to improved guidance on the future conditions of ENSO and the SIOD, provide optimism for seasonal prediction of Southern Africa precipitation (Yuan et al. 2014), where SST play a critical role in the regional climate. Therefore, the information presented here can be used alongside improved statistical and dynamical forecasts to make more informed Southern Africa precipitation forecasts during the December-March rainy season.

Acknowledgements

The authors thank Dave Allured for completing the ECHAM5.4 simulations and Tao Zhang for completing the GFSv2 simulations. The authors are grateful for support from the Famine Early Warning Systems Network (FEWS NET).

References

Adler, R. F., and Coauthors, 2003: The Version-2 Global Precipitation Climatology Project (GPCP) Monthly Precipitation Analysis (1979–Present). Journal of Hydrometeorology, 4, 1147-1167.

Allan, R. J., C. J. C. Reason, J. A. Lindesay, and T. J. Ansell, 2003: Protracted' ENSO episodes and their impacts in the Indian Ocean region. Deep Sea Research Part II: Topical Studies in Oceanography, 50, 2331-2347.

Behera, S. K., J.-J. Luo, S. Masson, P. Delecluse, S. Gualdi, A. Navarra, and T. Yamagata, 2005: Paramount Impact of the Indian Ocean Dipole on the East African Short Rains: A CGCM Study. Journal of Climate, 18, 4514-4530.

Behera, S. K., P. S. Salvekar, and T. Yamagata, 2000: Simulation of Interannual SST Variability in the Tropical Indian Ocean. Journal of Climate, 13, 3487-3499.

Behera, S. K., and T. Yamagata, 2001: Subtropical SST dipole events in the southern Indian Ocean. Geophysical Research Letters, 28, 327-330.

Chambers, D. P., B. D. Tapley, and R. H. Stewart, 1999: Anomalous warming in the Indian Ocean coincident with El Niño. Journal of Geophysical Research: Oceans, 104, 3035-3047.

Fauchereau, N., B. Pohl, C. J. C. Reason, M. Rouault, and Y. Richard, 2008: Recurrent daily OLR patterns in the Southern Africa/Southwest Indian Ocean region, implications for South African rainfall and teleconnections. Clim Dyn, 32, 575-591.

Goddard, L., and N. E. Graham, 1999: Importance of the Indian Ocean for simulating rainfall anomalies over eastern and southern Africa. Journal of Geophysical Research: Atmospheres, 104, 19099-19116.

Grove, C. A., Zinke, J., Peeters, F., Park, W., Scheufen, T., Kasper, S., Randriamanantsoa, B., McCulloch, M. T. and Brummer, GJA 2012. Madagascar corals reveal Pacific multidecadal modulation of rainfall since 1708. *Climate of the Past* 9, 641-656.

Hansingo, K., and C. J. C. Reason, 2009: Modelling the atmospheric response over southern Africa to SST forcing in the southeast tropical Atlantic and southwest subtropical Indian Oceans. International Journal of Climatology, 29, 1001-1012.

Hastenrath, S., L. Greischar, and J. van Heerden, 1995: Prediction of the Summer Rainfall over South Africa. Journal of Climate, 8, 1511-1518.

Hoell, A., C. Funk, T. Magadzire, J. Zinke, and G. Husak, 2015: El Niño–Southern Oscillation diversity and Southern Africa teleconnections during Austral Summer. Clim Dyn, 45, 1583-1599.

Huffman, G. J., R. F. Adler, D. T. Bolvin, and G. Gu, 2009: Improving the global precipitation record: GPCP Version 2.1. Geophysical Research Letters, 36, n/a-n/a.

Hurrell, J. W., J. J. Hack, D. Shea, J. M. Caron, and J. Rosinski, 2008: A New Sea Surface Temperature and Sea Ice Boundary Dataset for the Community Atmosphere Model. Journal of Climate, 21, 5145-5153.

Jury, M. R., 1992: A Climatic Dipole Governing the Interannual Variability of Convection over the SW Indian Ocean and SE Africa Region. Trends Geophys Res, 1, 165-172.

Jury, M. R., C. Mc Queen, and K. Levey, 1994: SOI and QBO signals in the African region. Theor Appl Climatol, 50, 103-115.

Landman, W. A., D. DeWitt, D.-E. Lee, A. Beraki, and D. Lötter, 2011: Seasonal Rainfall Prediction Skill over South Africa: One- versus Two-Tiered Forecasting Systems. Weather and Forecasting, 27, 489-501.

Landman, W. A., and L. Goddard, 2005: Predicting southern African summer rainfall using a combination of MOS and perfect prognosis. Geophysical Research Letters, 32, n/a-n/a.

Lindesay, J. A., 1988: South African rainfall, the Southern Oscillation and a Southern Hemisphere semi-annual cycle. Journal of Climatology, 8, 17-30.

Lyon, B., and S. J. Mason, 2009: The 1997/98 Summer Rainfall Season in Southern Africa. Part II: Model Simulations and Coupled Model Forecasts. Journal of Climate, 22, 3802-3818.

Manatsa, D., C. H. Matarira, and G. Mukwada, 2011: Relative impacts of ENSO and Indian Ocean dipole/zonal mode on east SADC rainfall. International Journal of Climatology, 31, 558-577.

Manatsa, D., T. Mushore, and A. Lenouo, 2015: Improved predictability of droughts over southern Africa using the standardized precipitation evapotranspiration index and ENSO. Theor Appl Climatol, 1-16.

Manatsa, D., C. J. C. Reason, and G. Mukwada, 2012: On the decoupling of the IODZM from southern Africa Summer rainfall variability. International Journal of Climatology, 32, 727-746.

Mason, S. J., and M. R. Jury, 1997: Climatic variability and change over southern Africa: a reflection on underlying processes. Progress in Physical Geography, 21, 23-50.

Misra, V., 2003: The Influence of Pacific SST Variability on the Precipitation over Southern Africa. Journal of Climate, 16, 2408-2418.

Nicholson, S., and D. Entekhabi, 1986: The quasi-periodic behavior of rainfall variability in Africa and its relationship to the southern oscillation. Arch. Met. Geoph. Biocl. A., 34, 311-348.

Nicholson, S. E., 1997: AN ANALYSIS OF THE ENSO SIGNAL IN THE TROPICAL ATLANTIC AND WESTERN INDIAN OCEANS. International Journal of Climatology, 17, 345-375.

Nicholson, S. E., and J. Kim, 1997: THE RELATIONSHIP OF THE EL NIÑO–SOUTHERN OSCILLATION TO AFRICAN RAINFALL. International Journal of Climatology, 17, 117-135.

Ratnam, J. V., S. K. Behera, Y. Masumoto, and T. Yamagata, 2014: Remote Effects of El Niño and Modoki Events on the Austral Summer Precipitation of Southern Africa. Journal of Climate, 27, 3802-3815.

Reason, C., 2015: Tropical South East Atlantic Warm Events and Associated Rainfall Anomalies over southern Africa. Frontiers in Environmental Science, 3.

Reason, C. J. C., 2001: Subtropical Indian Ocean SST dipole events and southern African rainfall. Geophysical Research Letters, 28, 2225-2227.

Reason, C. J. C., R. J. Allan, J. A. Lindesay, and T. J. Ansell, 2000: ENSO and climatic signals across the Indian Ocean Basin in the global context: part I, interannual composite patterns. International Journal of Climatology, 20, 1285-1327.

Reason, C. J. C., and D. Jagadheesha, 2005: A model investigation of recent ENSO impacts over southern Africa. Meteorol. Atmos. Phys., 89, 181-205.

Reason, C. J. C., and M. Rouault, 2002: ENSO-like decadal variability and South African rainfall. Geophysical Research Letters, 29, 16-11-16-14.

Rocha, A., and I. A. N. Simmonds, 1997: INTERANNUAL VARIABILITY OF SOUTH-EASTERN AFRICAN SUMMER RAINFALL. PART 1: RELATIONSHIPS WITH AIR–SEA INTERACTION PROCESSES. International Journal of Climatology, 17, 235-265.

Roeckner, E., and Coauthors, 2006: Sensitivity of Simulated Climate to Horizontal and Vertical Resolution in the ECHAM5 Atmosphere Model. Journal of Climate, 19, 3771-3791.

Rouault, M., P. Florenchie, N. Fauchereau, and C. J. C. Reason, 2003: South East tropical Atlantic warm events and southern African rainfall. Geophysical Research Letters, 30, n/a-n/a.

Saha, S., and Coauthors, 2013: The NCEP Climate Forecast System Version 2. Journal of Climate, 27, 2185-2208.

Saji, N. H., B. N. Goswami, P. N. Vinayachandran, and T. Yamagata, 1999: A dipole mode in the tropical Indian Ocean. Nature, 401, 360-363.

Saji, N. H., and T. Yamagata, 2003: Possible impacts of Indian Ocean Dipole mode events on global climate. Climate Research, 25, 151-169.

Wang, B., and Coauthors, 2009: Advance and prospectus of seasonal prediction: assessment of the APCC/CliPAS 14-model ensemble retrospective seasonal prediction (1980–2004). Clim Dyn, 33, 93-117.

Washington, R., and A. Preston, 2006: Extreme wet years over southern Africa: Role of Indian Ocean sea surface temperatures. Journal of Geophysical Research: Atmospheres, 111, n/a-n/a.

Webster, P. J., A. M. Moore, J. P. Loschnigg, and R. R. Leben, 1999: Coupled ocean-atmosphere dynamics in the Indian Ocean during 1997-98. Nature, 401, 356-360.

Wyrtki, K., 1975: El Niño—The Dynamic Response of the Equatorial Pacific Oceanto Atmospheric Forcing. Journal of Physical Oceanography, 5, 572-584.

Yuan, C., T. Tozuka, W. Landman, and T. Yamagata, 2014: Dynamical seasonal prediction of Southern African summer precipitation. Clim Dyn, 42, 3357-3374.

Zinke, J., Pfeiffer, M., Timm, O., Dullo, W.-Chr. and Brummer, G. J. A. 2009. Western Indian Ocean marine and terrestrial records of climate variability: a review and new concepts on land-ocean interaction since A.D. 1660. International Journal of Earth Sciences 98, Special Volume. doi:10.007/s00531-008-0365-5.

List of Tables

Table 1: ENSO and SIOD phase combinations for December-March 1979-2014. El Niño (La Niña) events are defined when the December-March Niño3.4 index anomaly exceeds (falls below) 0.5K (-0.5K).

	El Niño	La Niña
Negative SIOD	1982-1983, 1991-1992, 1994-1995, 1997-1998, 2002-2003, 2009-2010	1983-1984, 1984-1985, 1985-1986, 1988-1989, 1995-1996, 1999-2000, 2011-2012
Positive SIOD	1986-1987, 1987-1988, 2004-2005, 2006-2007	1998-1999, 2000-2001, 2005-2006, 2007-2008, 2008-2009, 2010-2011

List of Figures

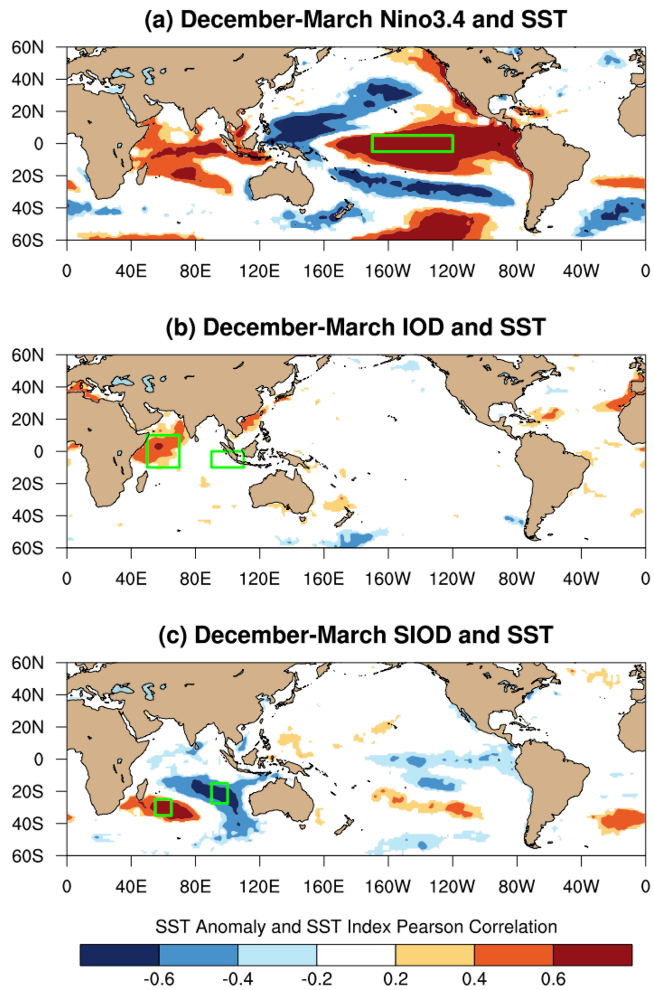

Figure 1: Correlation of December-March 1979-2014 SST anomaly and (a) the Niño3.4 index anomaly, (b) the IOD index anomaly and (c) the SIOD index anomaly. Shading indicates correlations significant at $p<0.10$. The Niño3.4 index is defined as areal average SST over 5°S-5°N; 170°W-120°W shown as the green outline in panel (a). The IOD index is defined as areal average SST over 10°S-0°N; 90°E-110°E subtracted from areal average SST over 10°S-10°N; 50°E-70°E, both of which are shown as green outlines on panel (b). The SIOD index is defined as areal average SST over 28°S-18°N; 90°E-100°E subtracted from areal average SST over 37°S-27°S; 55°E-65°E, both of which are shown as green outlines on panel (c).

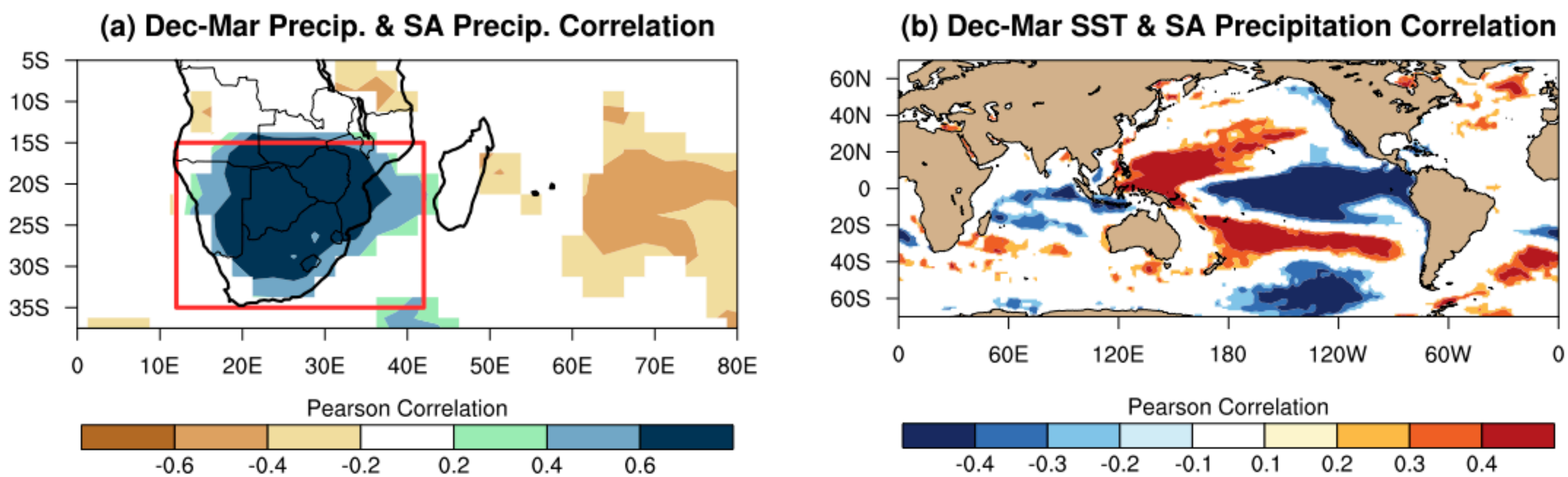

Figure 2: December-March 1979-2014 correlation of observed Southern Africa precipitation anomaly with (a) observed spatial precipitation anomaly and (b) observed SST anomaly. Shading indicates correlations significant at $p<0.10$.

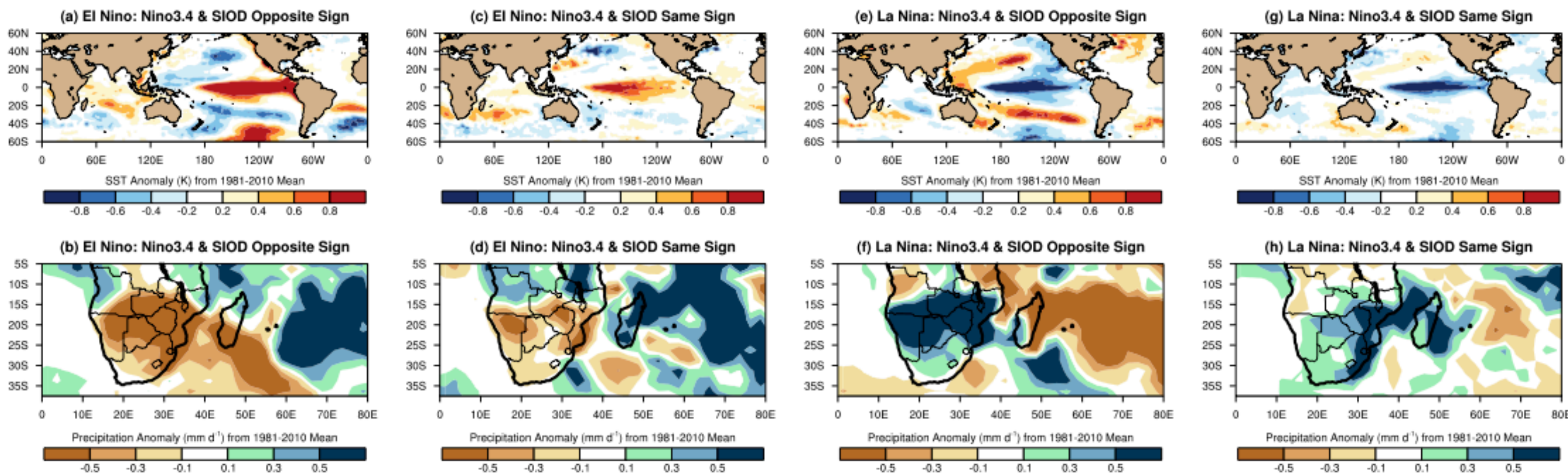

Figure 3: December-March (top) SST anomaly in units of K and (bottom) precipitation anomaly in units of mm d^{-1} during El Niño and La Niña events in which the Niño3.4 index anomaly and SIOD index anomaly have the same and opposing signs. El Niño (La Niña) events are defined when the December-March Niño3.4 index anomaly exceeds (falls below) 0.5K (-0.5K).

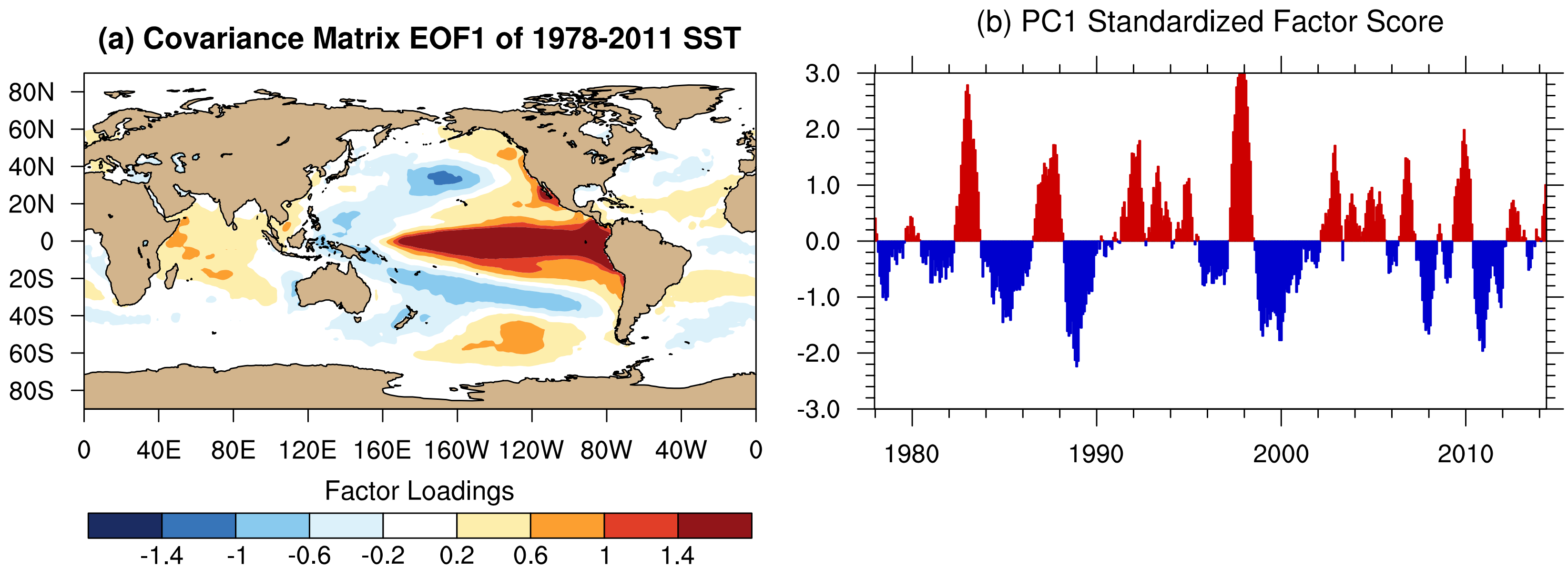

Figure 4: (a) The leading pattern of global SST anomaly in units of K calculated using a covariance-based empirical orthogonal function (EOF1) and (b) associated principal component for 1978-2014.

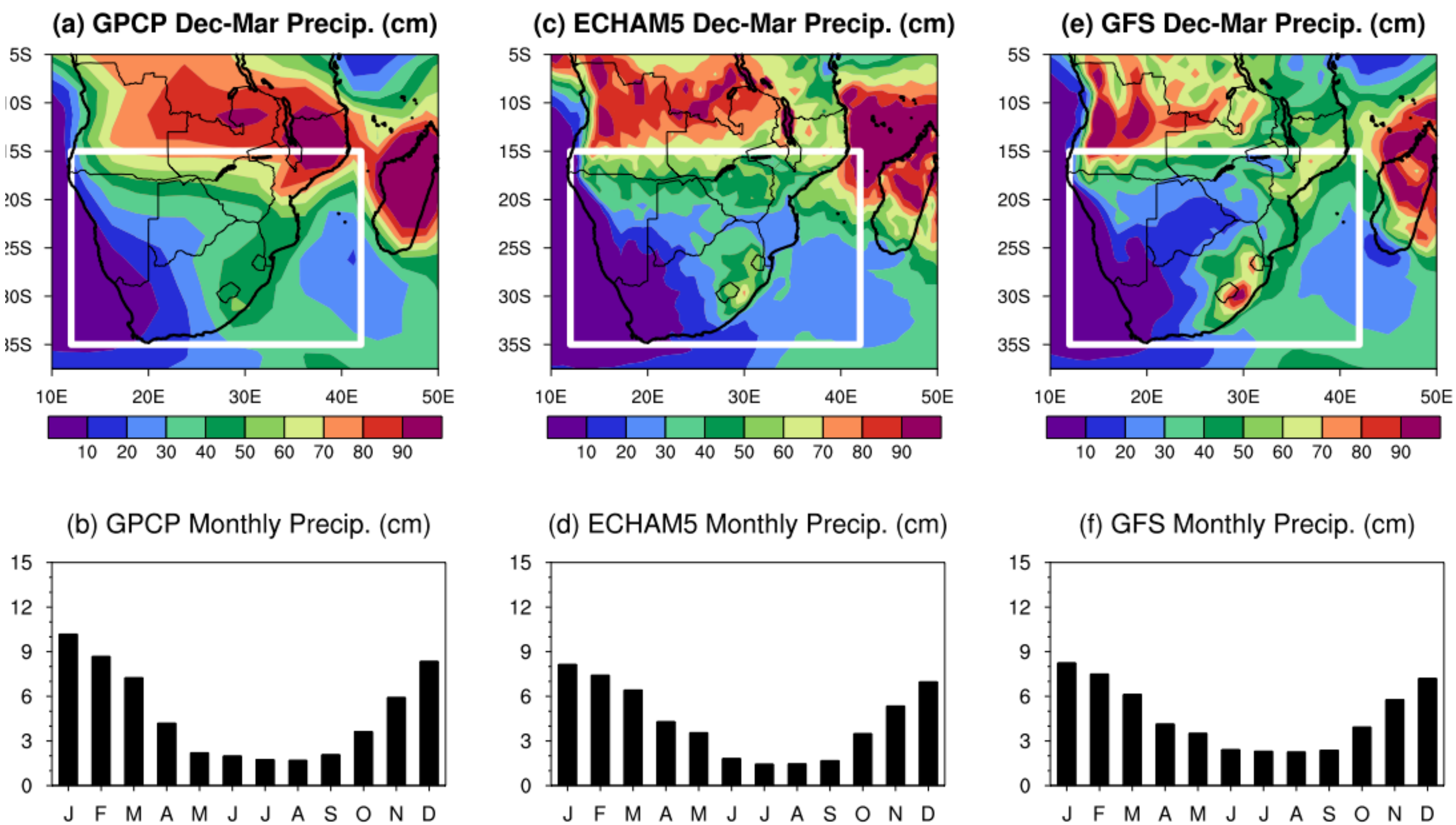

Figure 5: (top) December-March 1979-2014 average rainfall (cm) and (bottom) monthly average 1979-2014 rainfall (cm) in (left column) GPCP, (center column) 30 ECHAM5.4 simulations and (right column) 50 GFS version 2 simulations driven by global SST.

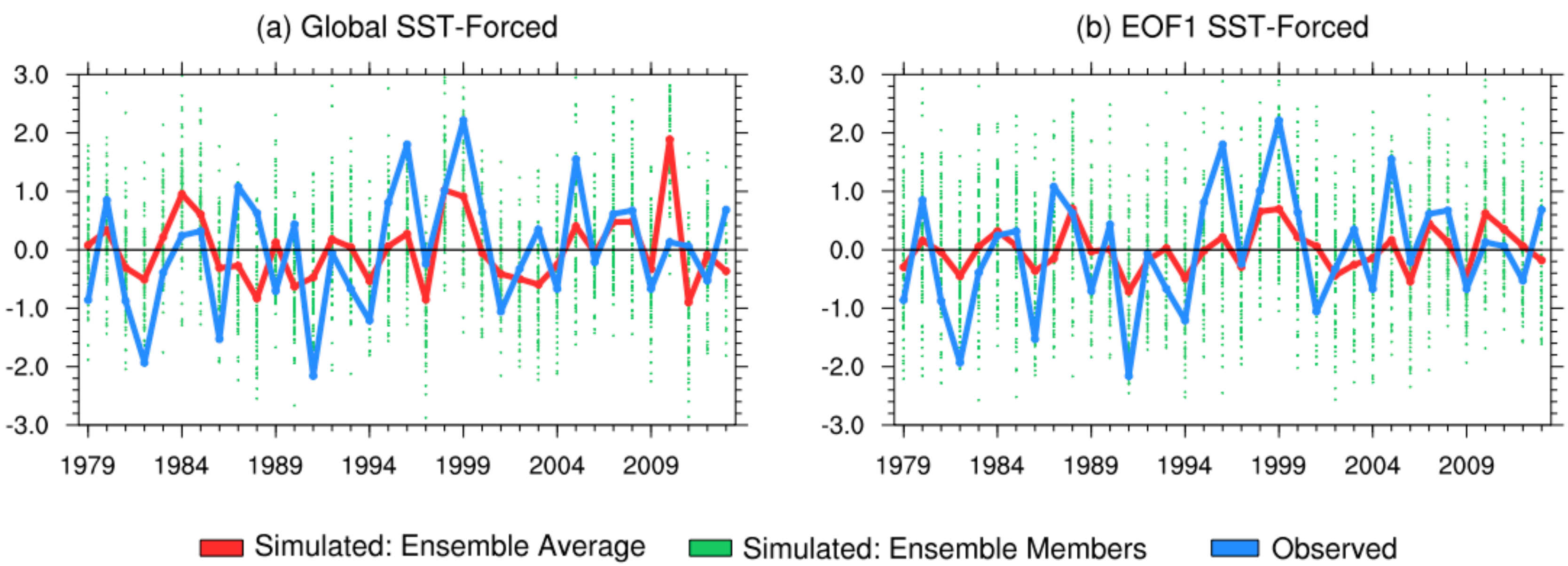

Figure 6: Simulated December-March 1979-2014 standardized Southern Africa precipitation anomaly forced by (a) global SST and (b) EOF1 of SST. Green dots indicate individual simulated ensembles, the red line shows the simulated ensemble average and the blue line shows observed precipitation.

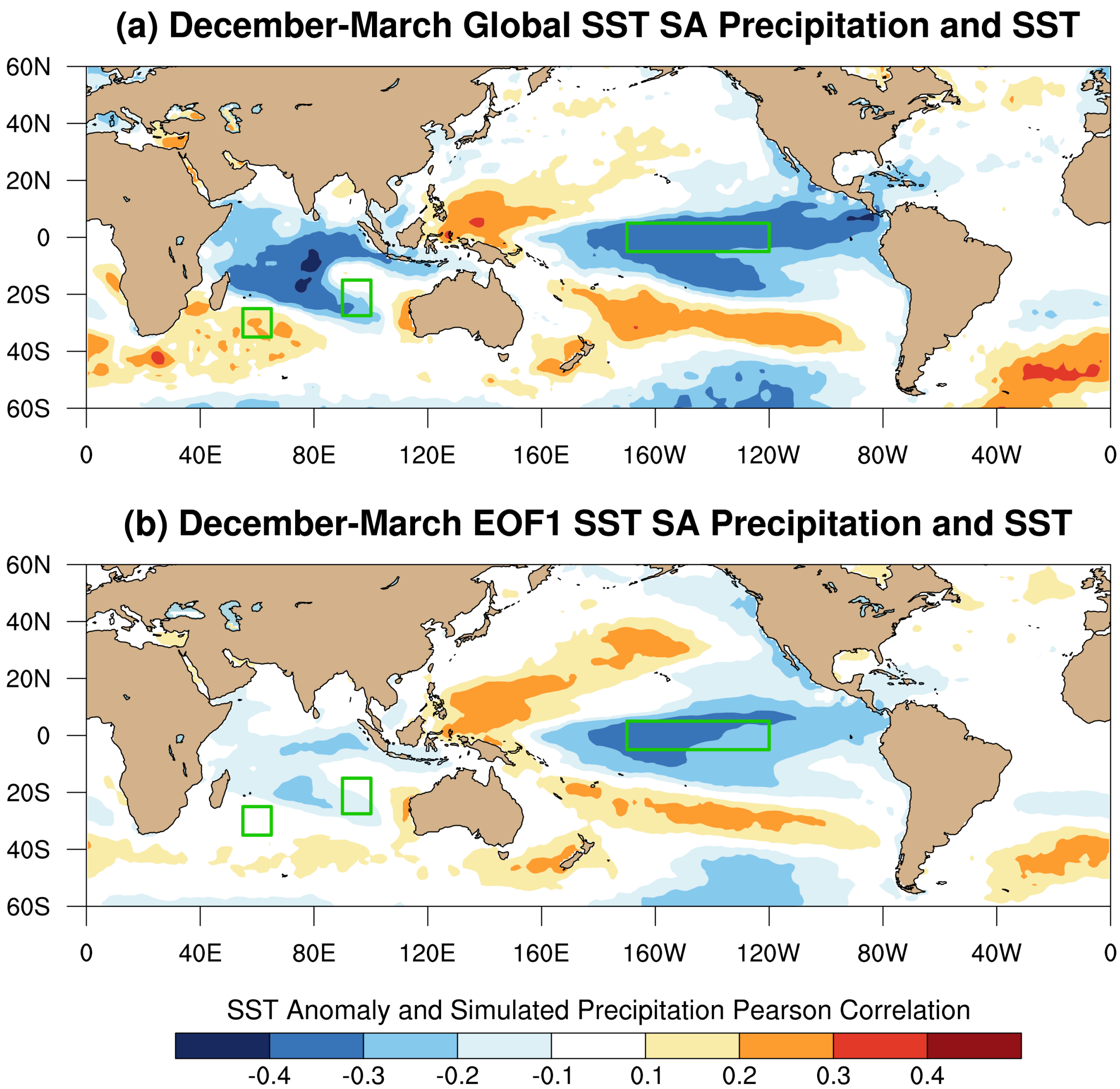

Figure 7: December-March 1979-2014 correlation of observed SST anomaly and simulated precipitation forced by (a) global SST and (b) EOF1 of SST. Shading denotes correlations significant at $p<0.10$.

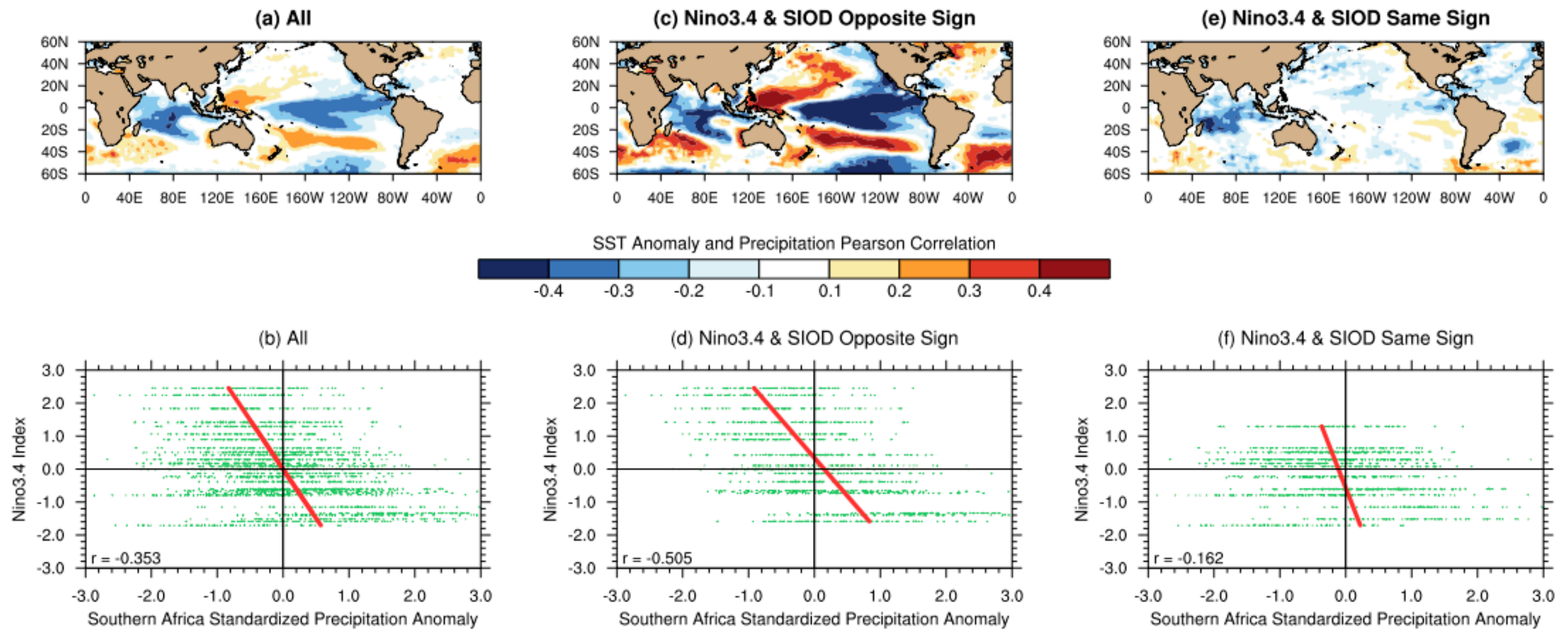

Figure 8: (top row) Correlation of simulated Southern Africa standardized precipitation anomaly forced by global SST with global SST. (bottom row) Scatter diagrams of observed Niño3.4 anomaly and simulated Southern Africa standardized precipitation anomaly forced by global SST (green dots) with the least squares regression line shown in red. Results are for December-March 1979-2014 and are shown (left column) in aggregate, (center column) when the Niño3.4 and SIOD indices have the opposite sign and (right column) when the Niño3.4 and SIOD indices have the same sign. Shading denotes correlations significant at $p<0.10$.

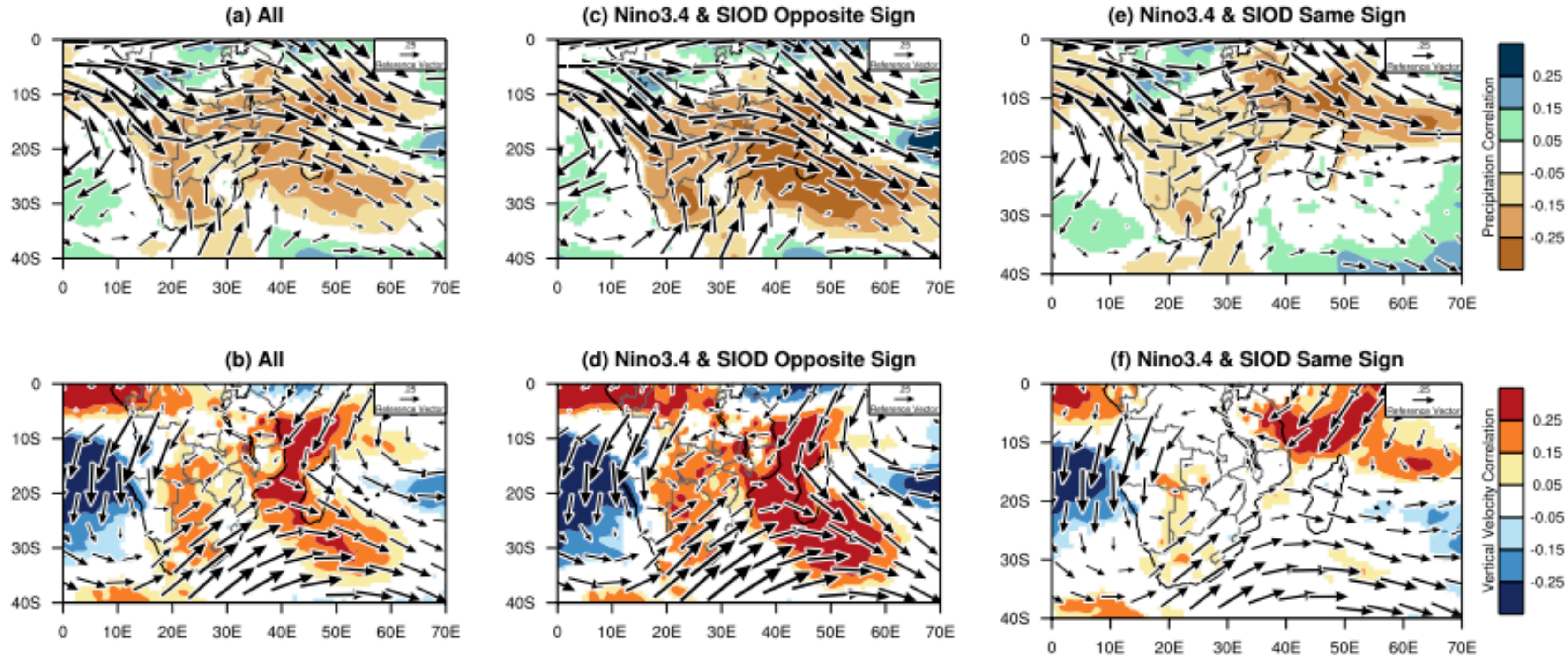

Figure 9: Correlation of Niño3.4 anomaly and simulated global SST-forced (top) 200 hPa wind anomaly (vector) and standardized precipitation anomaly (shading) and (bottom) 700 hPa wind anomaly (vector) and 400 hPa vertical velocity anomaly (shading) for December-March 1979-2014 (left column) in aggregate, (center column) when the Niño3.4 and SIOD indices have the opposite sign and (right column) when the Niño3.4 and SIOD indices have the same sign. Shading denotes correlations significant at $p<0.10$.

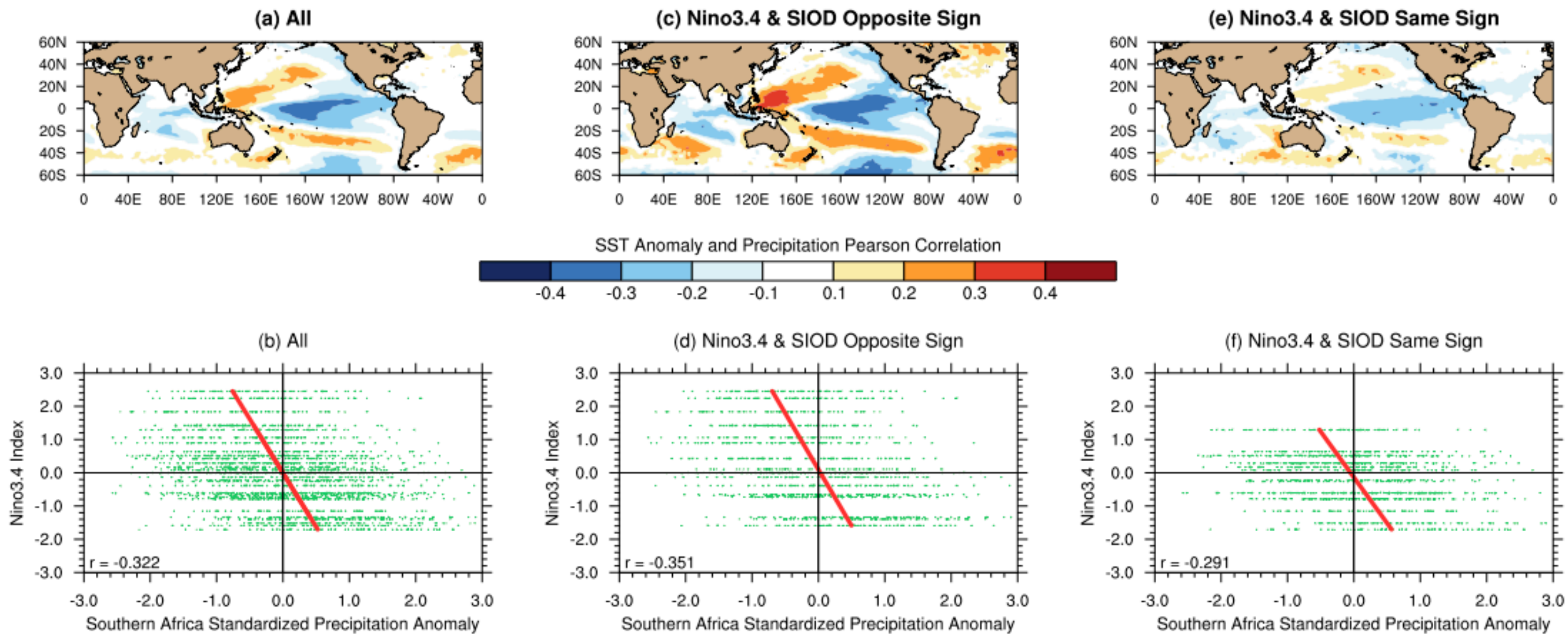

Figure 10: (top row) Correlation of simulated Southern Africa standardized precipitation anomaly forced by EOF1 with global SST. (bottom row) Scatter diagrams of observed Niño3.4 anomaly and simulated Southern Africa standardized precipitation anomaly forced by EOF1 (green dots) with the least squares regression line shown in red. Results are for December-March 1979-2014 and are shown (left column) in aggregate, (center column) when the Niño3.4 and SIOD indices have the opposite sign and (right column) when the Niño3.4 and SIOD indices have the same sign. Shading denotes correlations significant at $p<0.10$.

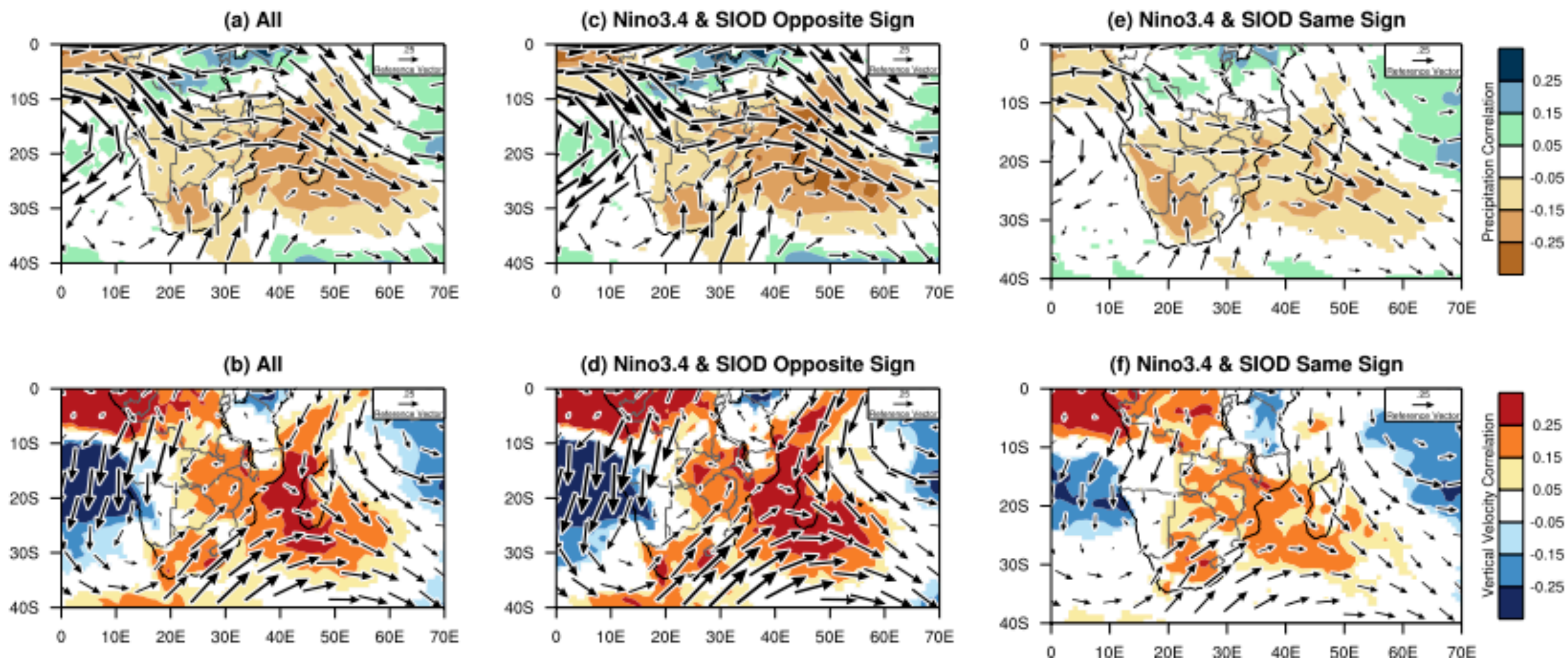

Figure 11: Correlation of Niño3.4 anomaly and simulated EOF1-forced (top) 200 hPa wind anomaly (vector) and standardized precipitation anomaly (shading) and (bottom) 700 hPa wind anomaly (vector) and 400 hPa vertical velocity anomaly (shading) for December-March 1979-2014 (left column) in aggregate, (center column) when the Niño3.4 and SIOD indices have the opposite sign and (right column) when the Niño3.4 and SIOD indices have the same sign. Shading denotes correlations significant at $p<0.10$.